Med Chem Res (2015) 24:588–602
DOI 10.1007/s00044-014-1152-4

MEDICINAL CHEMISTRY RESEARCH

ORIGINAL RESEARCH

Synthesis, docking and biological evaluation of oxamide and fumaramide analogs as potential AChE and BuChE inhibitors

Kadir Ozden Yerdelen · Edip Tosun

Received: 16 January 2014 / Accepted: 2 July 2014 / Published online: 20 July 2014

Abstract A new series of oxamide (**2a–s**) and fumaramide derivatives (**3a–s**) was synthesized and evaluated as acetylcholinesterase (AChE) and butyrylcholinesterase (BuChE) inhibitors against Alzheimer's disease (AD). Their inhibitory ability was compared to chosen reference compounds (galantamine bromide, neostigmine bromide, and ambenonium dichloride). Lineweaver–Burk plot and molecular docking studies showed that one of the most potent compounds **3o** ($IC_{50} = 0.03$ μM) could bind to both catalytic and peripheral active sites of AChE and it exhibited mixed-type inhibition. Moreover, it showed excellent metal chelating properties. The ethylene bridge, as the linker between the two carbonyl groups of the fumaramide derivatives, seemed to allow the fumaramide derivatives to be more effective than the oxamide derivatives on AChE inhibition. A similar situation was seen on BuChE inhibition, except for **2a** and **2h**. These results imply that the presence of an ethylene bridge in the inhibitors had more influence on the inhibition of AChE and BuChE.

Keywords Oxamide · Fumaramide · AChE · BuChE · Molecular docking

Introduction

Alzheimer's disease (AD), the most common form of dementia, is a complex neurodegenerative disorder occurring in the central nervous system (CNS), characterized by progressive cognitive decline, memory loss and learning and behavioral disturbances. AD primarily affects the elderly section of the population, specifically people aged 65 or older (Piazzi *et al*., 2003; Naj *et al*., 2011; Seshadri *et al*., 2010; Lambert *et al*., 2009). The significance of AD is further compounded, as the number of identified cases is estimated to quadruple by the year 2050 (Brookmeyer *et al*., 2007). The definite reason of the AD is still ambiguous, but in general the following hypothesis has been put forward on the basis of the various causative factors such as cholinergic, amyloid, tau, and metal hypothesis (Singh *et al*., 2013). The cholinergic hypothesis is one of the oldest and most popular hypothesis outlining the pathogenesis of AD. According to the cholinergic hypothesis, the main objective of current pharmacotherapy for AD are drugs intended to raise the levels of acetylcholine (ACh) by the inhibition of cholinesterase enzymes (ChEs) (Tai *et al*., 2012; Akasofu *et al*., 2008; Dumas and Newhouse, 2011). Studies have shown that AD is defined by the rapid loss of acetylcholinesterase (AChE) activity in the early stages of the disease, along with the increasing ratio of AChE as the disease progresses (Darvesh *et al*., 2003; Greig *et al*., 2005).

Two forms of the ChE enzymes, AChE and butyrylcholinesterase (BuChE), are localized within the cholinergic regions of the CNS. Both enzymes are able to hydrolyze ACh, but AChE has a 10^{13}-fold higher hydrolytic ACh activity than does BuChE under the same conditions (Skrzypek *et al*., 2013). In addition, BuChE has been found capable of compensating for the missing AChE catalytic functions in the synaptic cleft and its activity increases, 30–60 %, during AD (Jhee *et al*., 2002; Bullock and Lane, 2007; Mesulam *et al*., 2002; Kamal *et al*., 2008). Due to the role of BuChE in hydrolysis of ACh, inhibition of both cholinesterase enzymes using a dual inhibitor should

K. O. Yerdelen (✉) · E. Tosun
Department of Pharmaceutical Chemistry, Faculty of Pharmacy, Ataturk University, 25240 Erzurum, Turkey
e-mail: dadasozden@gmail.com

results in the increased levels of ACh in the brain that provides more successful clinical efficacy of AD (Khoobi *et al*., 2013; Basiri *et al*., 2013).

The structural character of AChE shows that the catalytic anionic site (CAS) is located at the bottom of a narrow 20-Å-deep gorge. Besides, the entrance of the gorge as a regulatory site is termed the peripheral anionic site (PAS) (Xinga *et al*., 2013). ChE inhibitors (ChEI) may inhibit both cholinesterase enzymes via a competitive mechanism, by interacting with the CAS, via a non-competitive mechanism, by binding with the PAS, or via mixed-type mechanisms, by exerting a dual binding ChE inhibition (Samadi *et al*., 2012).

Recent studies have indicated that another approach, called metal hypothesis, may contribute to AD pathology (Liu *et al*., 2006). The level of metal ions (Fe^{2+}, Cu^{2+}, Zn^{2+}) in AD patients is 3–7 times higher than in healthy individuals (Zatta *et al*., 2009). The excessive accumulation of metals increases the formation of beta-amyloid fibril aggregates, which induce inflammation and activate neurotoxic pathways, leading to the dysfunction and death of brain cells (Opazo *et al*., 2002; Dong *et al*., 2003; Yan *et al*., 2013). Thus, metal chelation therapy aimed at precluding and scavenging the occurrence of free radical metals may be considered a promising clinical approach to AD. Heavy metals, such as Cu^{2+}, Fe^{2+} and Zn^{2+}, may contribute to the production of reactive oxygen species and oxidative stress (Huang *et al*., 2004). Therefore, chelators, such as clioquinol, a specific Cu^{2+} and Zn^{2+} chelators been recommended as potential therapeutic treatments for AD (Bush, 2008; Ritchie *et al*., 2003).

Several anti-cholinesterase agents, such as rivastigmine (Exelon), galantamine (Razadyne), and donepezil (Aricept), only offer symptomatic relief without any disease-modifying effects. Unfortunately, these inhibitors have many side effects. One in particular, tacrines been shown to have a serious hepatotoxic effect (Sugimoto, 2008; Smith *et al*., 1997). In the view of the above mentioned reasons, we focused on the development of more active and selective dual inhibitors which are capable of interacting with the CAS and PAS of both ChEs.

α,β-unsaturated carbonyl-based compounds were obtained and evaluated for their cholinesterase inhibition capacity. Some of these compounds exhibited a respectable activity on AChE and BuChE inhibition with the half maximal inhibitory concentration (IC_{50}) values in the micromolar (μM) ranges (Hasan *et al*., 2005; Yerdelen and Gul, 2013). In this study, a new series of oxamide and fumaramide derivatives was synthesized, evaluated and molecularly modeled. The pharmacological evaluations of these new compounds included AChE and BuChE inhibition, the kinetics of enzyme inhibition and metal chelation. Finally, molecular modeling studies were performed to understand the interactions between the related enzyme and the most potent compounds.

Materials and methods

Chemistry

The ^{1}H and ^{13}C nuclear magnetic resonance (NMR) spectra were recorded with tetramethylsilane (TMS) as the internal standard on a Bruker FT-400(100) MHz spectrometer using $CDCl_3$ as the solvent. Coupling constants were given in Hertz (Hz). Mass (LC-MS) spectra were recorded on Agilent 1200 mass spectrometer at 10 eV. Melting points of the compounds were obtained on Electrothermal 9100 melting-point apparatus. Benzaniline compounds were synthesized with CEM 3100 microwave oven. Reaction progress and product mixtures were routinely checked by thin-layer chromatography (TLC) on Merck SilicaGel F254 aluminum plates. Column chromatography was performed with SiO_2 (70–230 mesh). The chemical reagents and solvents used in this study were purchased from Merck or Sigma Aldrich.

General synthesis procedure under solvent-free phase-transfer catalysis conditions (**1a**–**s**)

A mixture of meta-substituted aniline (10 mmol), benzyl chloride, or *p*-methylbenzyl chloride (5 mmol) was adsorbed on a mixture of potassium carbonate (6.25 mmol) and tetrabutylammonium bromide (1 mmol) and then the resulting fine powder was irradiated with CEM microwave (150 W, 120 °C) for 5 min. Completion of the reaction was checked by TLC and all of the compounds were purified by column chromotography on silica gel with hexane:ethyl acetate (9:1) mobile phase. Synthesis pathway is shown on Scheme 1.

A general procedure for the synthesis of oxamide compounds (**2a**–**s**)

A mixture of the meta-substituted benzaniline (1.3 mmol), triethylamine (TEA) (1.3 mmol), and oxalyl chloride (0.66 mmol) in tetrahydrofuran (5 mL) was stirred at room temperature for 12 h. The reaction mixture was quenched with 15 mL of distilled water and the aqueous phase was extracted with two portions of CH_2Cl_2. The combined organic layers were dried over $MgSO_4$, filtered and concentrated. The crude product was purified by column chromatography on silica gel with hexane:ethyl acetate (7:3) mobile phase. The obtained solid was recrystallized from EtOH.

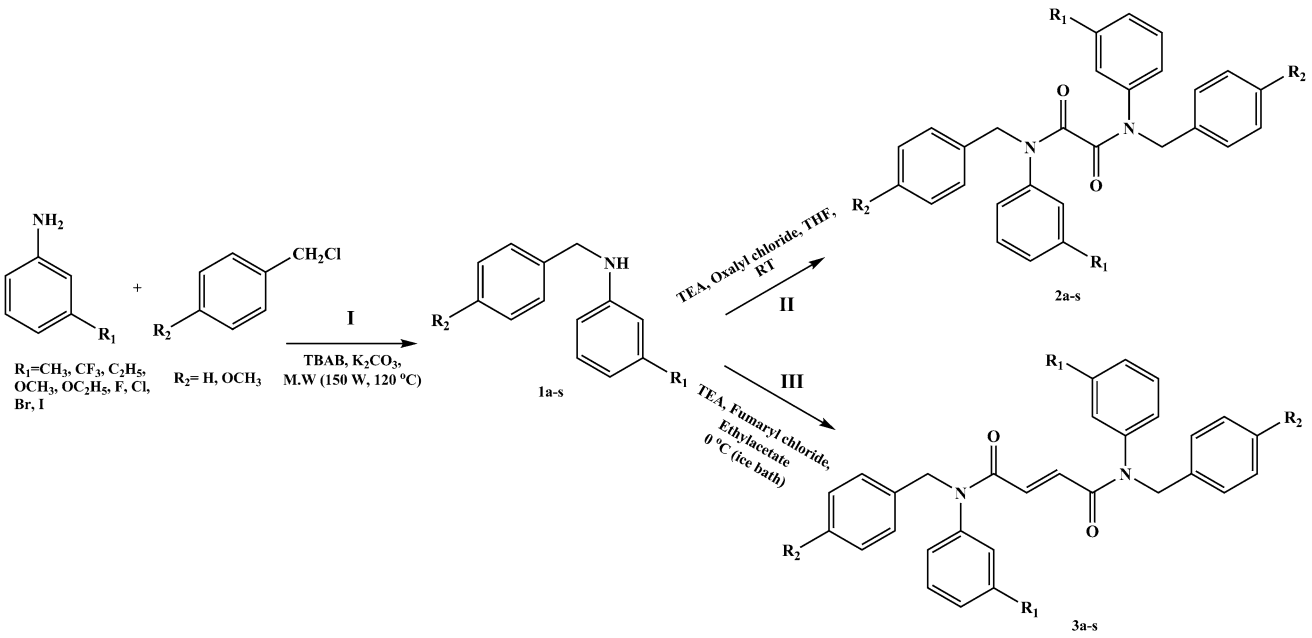

Scheme 1 Synthesis of the target compounds **2a–s** and **3a–s**

*N^1,N^2-dibenzyl-N^1,N^2-di-m-tolyl-oxamide (**2a**)*

Intermediate 3-methyl-*N*-(benzyl)aniline was reacted with oxalyl chloride following the general procedure to give the product **2a** as a white solid with a yield of 45 %; mp 152–155 °C. ^{1}H NMR (400 MHz, $CDCl_3$): δ ppm 2.28 (s, 6H, 2× CH_3), 4.80 (s, 4H, 2× CH_2-N), 6.78–6.76 (d, 2H, $J = 8.0$ Hz), 6.95 (s, 2H), 7.06–7.04 (d, 4H, $J = 7.7$ Hz), 7.11–7.09 (m, 2H), 7.18–7.14 (m, 6H), 7.36–7.34 (d, 2H, $J = 7.9$ Hz). ^{13}C NMR (100 MHz, $CDCl_3$): δ ppm 20.32 (Ph-CH_3), 53.24 (CH_2-N), 124.28, 128.48, 128.49, 128.55, 129.16, 129.87, 131.35, 136.22, 138.75, 140.42, 158.01 (C=O). ESI-MS *m/z* [M + H] = 449.5.

*N^1,N^2-bis-(4-methyl-benzyl)-N^1,N^2-di-m-tolyl-oxamide (**2b**)*

Intermediate 3-methyl-*N*-(4-methylbenzyl)aniline was reacted with oxalyl chloride following the general procedure to give the product **2b** as a white solid with a yield of 40 %; mp 148–152 °C. ^{1}H NMR (400 MHz, $CDCl_3$): δ ppm 2.23 (s, 6H), 2.28 (s, 6H), 4.80 (s, 4H, 2× CH_2-N), 6.72–6.70 (d, 2H, $J = 7.9$ Hz), 6.85 (s, 2H), 7.09 (bs, 8H), 7.15–7.13 (d, 2H, $J = 7.8$ Hz), 7.19–7.15 (m, 2H). ^{13}C NMR (100 MHz, $CDCl_3$): δ ppm 20.17 (*p*-CH_3), 22.31 (*m*-CH_3), 53.13 (CH_2-N), 124.98, 127.67, 129.56, 130.37, 133.26, 134.49, 137.22, 140.29, 140.56, 159.37 (C=O). ESI-MS *m/z* [M + H] = 477.6.

*N^1,N^2-dibenzyl-N^1,N^2-bis-(3-trifluoromethyl-phenyl)-oxamide (**2c**)*

Intermediate 3-trifluoromethyl-*N*-(benzyl)aniline was reacted with oxalyl chloride following the general procedure to give the product **2c** as a white solid with a yield of 57 %; mp 130–134 °C. ^{1}H NMR (400 MHz, $CDCl_3$): δ ppm 4.89 (s, 4H, 2× CH_2-N), 7.09–7.06 (m, 6H), 7.23–7.20 (m, 2H), 7.28–7.24 (m, 6H), 7.38–7.36 (d, 2H, $J = 7.7$ Hz), 7.58 (s, 2H). ^{13}C NMR (100 MHz, $CDCl_3$): δ ppm 51.25 (CH_2-N), 122.66, 126.12, 127.23, 129.31, 130.28, 132.02, 135.44, 139.65, 157.20 (C=O). ESI-MS *m/z* [M + H] = 557.5.

*N^1,N^2-bis-(4-methyl-benzyl)-N^1,N^2-bis-(3-trifluoromethyl-phenyl)-oxamide (**2d**)*

Intermediate 3-trifluoromethyl-*N*-(4-methylbenzyl)aniline was reacted with oxalyl chloride following the general procedure to give the product **2d** as a white solid with a yield of 42 %; mp 114–117 °C. ^{1}H NMR (400 MHz, $CDCl_3$): δ ppm 3.92 (s, 6H, 2× Ph-CH_3), 4.83 (s, 4H, 2× CH_2-N), 7.11–6.98 (d, 2H, $J = 7.9$ Hz), 7.01–6.99 (d, 4H, $J = 8.0$ Hz), 7.10–7.08 (d, 4H, $J = 7.7$ Hz), 7.24–7.22 (m, 2H), 7.34–7.32 (d, 2H, $J = 7.6$ Hz), 7.79 (s, 2H). ^{13}C NMR (100 MHz, $CDCl_3$): δ ppm 20.13 (Ph-CH_3), 52.56 (CH_2-N), 124.09, 128.63, 129.95, 130.48, 131.18, 135.36, 136.57, 139.92, 158.25 (C=O). ESI-MS *m/z* [M + H] = 585.2.

*N^1,N^2-dibenzyl-N^1,N^2-bis-(3-ethyl-phenyl)-oxamide (**2e**)*

Intermediate 3-ethyl-*N*-(benzyl)aniline was reacted with oxalyl chloride following the general procedure to give the product **2e** as a yellow oil with a yield of 82 %. ^{1}H NMR (400 MHz, $CDCl_3$): δ ppm 1.13–1.11 (t, 6H, 2× CH_2CH_3), 2.42–2.39 (q, 4H, 2× CH_2CH_3), 4.80 (s, 4H, 2× CH_2-N),

6.88–6.85 (d, 2H, $J = 7.6$ Hz), 7.05–7.01 (m, 6H), 7.18–7.14 (m, 6H), 7.21 (s, 2H). ^{13}C NMR (100 MHz, $CDCl_3$): δ ppm 18.45 (CH_2–*CH_3*), 27.38 (*CH_2*–CH_3), 52.64 (CH_2-N), 124.37, 126.99, 127.09, 128.24, 128.57, 131.23, 135.34, 140.78, 159.91 (C=O). ESI-MS *m/z* [M + H] = 477.6.

*N^1,N^2-bis-(3-ethyl-phenyl)-N^1,N^2-bis-(4-methyl-benzyl)-oxamide (**2f**)*

Intermediate 3-ethyl-*N*-(4-methylbenzyl)aniline was reacted with oxalyl chloride following the general procedure to give the product **2f** as a yellow oil with a yield of 59 %. ^{1}H NMR (400 MHz, $CDCl_3$): δ ppm 1.20–1.16 (t, 6H, 2× CH_2*CH_3*), 2.28 (s, 6H, 2× CH_3-Ph), 2.63–2.58 (q, 4H, 2× *CH_2*CH_3), 4.84 (s, 4H, 2× CH_2-N), 6.78–6.76 (bs, 4H), 7.03 (bs, 8H), 7.15–7.13 (d, 2H, $J = 7.69$ Hz), 7.26–7.21 (m, 2H). ^{13}C NMR (100 MHz, $CDCl_3$): δ ppm 13.33 (CH_2-*CH_3*), 20.42 (Ph-CH_3), 27.57 (*CH_2*-CH_3), 52.28 (CH_2-N), 125.03, 126.78, 127.02, 127.97, 128.69, 130.34, 133.51, 135.49, 139.32, 143.00, 160.32 (C=O). ESI-MS *m/z* [M + H] = 505.6.

*N^1,N^2-dibenzyl-N^1,N^2-bis-(3-methoxy-phenyl)-oxamide (**2g**)*

Intermediate 3-methoxy-*N*-(benzyl)aniline was reacted with oxalyl chloride following the general procedure to give the product **2g** as a white solid with a yield of 48 %; mp 152–155 °C. ^{1}H NMR (400 MHz, $CDCl_3$): δ ppm 2.28 (s, 6H, 2× OCH_3), 4.83 (s, 4H, 2× CH_2-N), 6.73–6.72 (d, 2H, $J = 7.6$ Hz), 6.90 (s, 2H), 7.11–7.09 (d, 4H, $J = 7.8$ Hz), 7.12–7.09 (m, 2H), 7.20–7.16 (m, 6H), 7.25–7.24 (d, 2H, $J = 7.8$ Hz). ^{13}C NMR (100 MHz, $CDCl_3$): δ ppm 20.19 (OCH_3), 52.67 (N-CH_2), 125.08, 126.25, 127.19, 128.11, 128.71, 131.37, 135.66, 137.84, 140.19, 161.23 (C=O). ESI-MS *m/z* [M + H] = 481.5.

*N^1,N^2-bis-(3-methoxy-phenyl)-N^1,N^2-bis-(4-methyl-benzyl)-oxamide (**2h**)*

Intermediate 3-methoxy-*N*-(4-methylbenzyl)aniline was reacted with oxalyl chloride following the general procedure to give the product **2h** as a yellow oil with a yield of 75 %. ^{1}H NMR (400 MHz, $CDCl_3$): δ ppm 2.21 (s, 6H, 2× Ph-CH_3), 3.68 (s, 6H, 2× OCH_3), 4.82 (s, 4H, 2× CH_2-N), 6.76–6.74 (d, 2H, $J = 7.7$ Hz), 6.91 (s, 2H), 7.10 (bs, 8H), 7.22–7.20 (d, 2H, $J = 7.6$ Hz), 7.23–7.20 (m, 2H). ^{13}C NMR (100 MHz, $CDCl_3$): δ ppm 20.12 (Ph-CH_3), 52.22 (OCH_3), 55.75 (N-CH_2), 111.65, 112.47, 119.49, 128.30, 130.11, 132.83, 135.73, 140.42, 153.92, 159.22 (C=O). ESI-MS *m/z* [M + H] = 509.6.

*N^1,N^2-dibenzyl-N^1,N^2-bis-(3-ethoxy-phenyl)-oxamide (**2i**)*

Intermediate 3-ethoxy-*N*-(benzyl)aniline was reacted with oxalyl chloride following the general procedure to give the product **2i** as a yellow solid with a yield of 77 %; mp 94–98 °C. ^{1}H NMR (400 MHz, $CDCl_3$): δ ppm 1.33–1.30 (t, 6H, 2× CH_2*CH_3*), 3.85–3.82 (q, 4H, 2× *CH_2*CH_3), 4.80 (s, 4H, 2× CH_2-N), 6.53–6.51 (d, 2H, $J = 7.8$ Hz), 6.90 (s, 2H), 7.08-7.05 (d, 4H, $J = 7.8$ Hz), 7.12–7.09 (m, 2H), 7.14–7.11 (m, 6H), 7.20–7.18 (d, 2H, $J = 8.0$ Hz). ^{13}C NMR (100 MHz, $CDCl_3$): δ ppm 15.03 (OCH_2*CH_3*), 52.57 (*OCH_2*CH_3), 60.11 (N-CH_2), 111.03, 119.89, 122.34, 125.43, 128.31, 130.99, 134.21, 139.31, 155.22, 159.28 (C=O). ESI-MS *m/z* [M + H] = 509.6.

*N^1,N^2-bis-(3-ethoxy-phenyl)-N^1,N^2-bis-(4-methyl-benzyl)-oxamide (**2j**)*

Intermediate 3-ethoxy-*N*-(4-methylbenzyl)aniline was reacted with oxalyl chloride following the general procedure to give the product **2j** as a orange solid with a yield of 87 %; mp 78–81 °C. ^{1}H NMR (400 MHz, $CDCl_3$): δ ppm 1.38–1.35 (t, 6H, 2× OCH_2*CH_3*), 2.20 (s, 6H, 2× CH_3), 3.86–3.83 (q, 4H, 2× *OCH_2*CH_3), 4.85 (s, 4H, 2× CH_2-N), 6.68 (s, 2H), 6.73–6.72 (d, 2H, $J = 8.1$ Hz), 6.81–6.78 (d, 2H, $J = 8.0$ Hz), 7.00–6.94 (bs, 8H), 7.23–7.19 (m, 2H). ^{13}C NMR (100 MHz, $CDCl_3$): δ ppm 15.23 (OCH_2*CH_3*), 20.11 (Ph-CH_3), 53.09 (*OCH_2*CH_3), 61.59 (N-CH_2), 112.89, 113.96, 119.22, 125.18, 128.35, 130.09, 131.57, 135.92, 140.01, 152.74, 159.94 (C=O). ESI-MS *m/z* [M + H] = 537.6.

*N^1,N^2-dibenzyl-N^1,N^2-bis-(3-fluoro-phenyl)-oxamide (**2k**)*

Intermediate 3-fluoro-*N*-(benzyl)aniline was reacted with oxalyl chloride following the general procedure to give the product **2k** as a white solid with a yield of 59 %; mp 155–159 °C. ^{1}H NMR (400 MHz, $CDCl_3$): δ ppm 4.82 (s, 4H, 2× CH_2-N), 6.88–6.86 (d, 2H, $J = 7.6$ Hz), 7.03–7.00 (m, 2H), 7.15–7.13 (d, 4H, $J = 7.8$ Hz), 7.25–7.22 (m, 6H), 7.30–7.28 (d, 2H, $J = 7.9$ Hz). ^{13}C NMR (100 MHz, $CDCl_3$): δ ppm 51.22 (N-CH_2), 112.11, 113.57, 121.00, 125.23, 128.61, 129.15, 131.62, 134.23, 140.21, 157.98, 159.11 (C=O). ESI-MS *m/z* [M + H] = 457.4.

*N^1,N^2-bis-(3-fluoro-phenyl)-N^1,N^2-bis-(4-methyl-benzyl)-oxamide (**2l**)*

Intermediate 3-fluoro-*N*-(4-methylbenzyl)aniline was reacted with oxalyl chloride following the general procedure to give the product **2l** as a white solid with a yield of 55 %; mp

112–115 °C. ^{1}H NMR (400 MHz, $CDCl_3$): δ ppm 2.21 (s, 6H, 2× CH_3), 4.81 (s, 4H, 2× CH_2-N), 6.78–6.70 (m, 4H), 7.01–6.98 (d, 4H, $J = 7.8$ Hz), 7.06–7.04 (d, 4H, $J = 8.0$ Hz), 7.28–7.25 (d, 2H, $J = 8.0$ Hz), 7.32–7.29 (m, 2H). ^{13}C NMR (100 MHz, $CDCl_3$): δ ppm 20.01 (Ph-CH_3), 52.24 (N-CH_2), 111.09, 112.47, 121.04, 125.35, 128.57, 129.90, 131.26, 135.21, 139.82, 157.25, 160.91 (C=O). ESI-MS m/z [M + H] = 485.6.

*N^1,N^2-dibenzyl-N^1,N^2-bis-(3-chloro-phenyl)-oxamide (**2m**)*

Intermediate 3-chloro-*N*-(benzyl)aniline was reacted with oxalyl chloride following the general procedure to give the product **2m** as a white solid with a yield of 44 %; mp 128–130 °C. ^{1}H NMR (400 MHz, $CDCl_3$): δ ppm 4.82 (s, 4H, 2× CH_2-N), 6.81–6.80 (d, 2H, $J = 7.9$ Hz), 7.00 (s, 2H), 7.25–7.24 (d, 4H, $J = 8.0$ Hz), 7.27–7.24 (m, 2H), 7.28–7.26 (m, 6H), 7.32–7.30 (d, 2H, $J = 8.0$ Hz). ^{13}C NMR (100 MHz, $CDCl_3$): δ ppm 52.45 (N-CH_2), 123.31, 125.64, 126.11, 127.25, 127.98, 129.14, 130.72, 131.67, 132.42, 138.38, 160.59 (C=O). ESI-MS m/z [M + H] = 490.3.

*N^1,N^2-bis-(3-chloro-phenyl)-N^1,N^2-bis-(4-methyl-benzyl)-oxamide (**2n**)*

Intermediate 3-chloro-*N*-(4-methylbenzyl)aniline was reacted with oxalyl chloride following the general procedure to give the product **2n** as a white solid with a yield of 57 %; mp 144–148 °C. ^{1}H NMR (400 MHz, $CDCl_3$): δ ppm 2.21 (s, 6H, 2× CH_3), 4.83 (s, 4H, 2× CH_2-N), 6.80 (s, 2H), 7.05 (bs, 8H), 7.06–7.04 (d, 2H, $J = 8.0$ Hz), 7.24–7.20 (m, 2H), 7.30–7.28 (d, 2H, $J = 7.5$ Hz). ^{13}C NMR (100 MHz, $CDCl_3$): δ ppm 20.34 (Ph-CH_3), 53.02 (N-CH_2), 113.28, 114.58, 121.15, 126.49, 128.21, 129.01, 130.59, 131.08, 135.22, 140.55, 158.23 (C=O). ESI-MS m/z [M + H] = 518.4.

*N^1,N^2-dibenzyl-N^1,N^2-bis-(3-bromo-phenyl)-oxamide (**2o**)*

Intermediate 3-bromo-*N*-(benzyl)aniline was reacted with oxalyl chloride following the general procedure to give the product **2o** as a white solid with a yield of 45 %; mp 114–119 °C. ^{1}H NMR (400 MHz, $CDCl_3$): δ ppm 4.85 (s, 4H, 2× CH_2-N), 6.83–6.81 (d, 2H, $J = 7.7$ Hz), 7.00 (s, 2H), 7.11–7.08 (d, 4H, $J = 7.8$ Hz), 7.25–7.24 (m, 2H), 7.30–7.27 (m, 6H), 7.36–7.34 (d, 2H, $J = 7.9$ Hz). ^{13}C NMR (100 MHz, $CDCl_3$): δ ppm 51.54 (N-CH_2), 121.10, 123.20, 125.54, 126.47, 129.11, 130.11, 130.91, 131.12, 133.27, 139.47, 158.77 (C=O). ESI-MS m/z [M + H] = 579.2.

*N^1,N^2-bis-(3-bromo-phenyl)-N^1,N^2-bis-(4-methyl-benzyl)-oxamide (**2p**)*

Intermediate 3-bromo-*N*-(4-methylbenzyl)aniline was reacted with oxalyl chloride following the general procedure to give the product **2p** as a white solid with a yield of 45 %; mp 146–149 °C. ^{1}H NMR (400 MHz, $CDCl_3$): δ ppm 2.31 (s, 6H, 2× CH_3), 4.81 (s, 4H, 2× CH_2-N), 6.85–6.83 (d, 2H, $J = 7.8$ Hz), 7.01–7.00 (d, 4H, $J = 8.1$ Hz), 7.04–7.01 (d, 4H, $J = 7.9$ Hz), 7.28 (s, 2H), 7.32–7.30 (d, 2H, $J = 8.1$ Hz), 7.44–7.41 (m, 2H). ^{13}C NMR (100 MHz, $CDCl_3$): δ ppm 20.44 (Ph-CH_3), 51.13 (N-CH_2), 120.24, 125.13, 127.45, 128.85, 130.13, 130.92, 131.21, 132.99, 133.42, 139.51, 159.46 (C=O). ESI-MS m/z [M + H] = 607.4.

*N^1,N^2-dibenzyl-N^1,N^2-bis-(3-iodo-phenyl)-oxamide (**2r**)*

Intermediate 3-iodo-*N*-(benzyl)aniline was reacted with oxalyl chloride following the general procedure to give the product **2r** as a white solid with a yield of 46 %; mp 138–142 °C. ^{1}H NMR (400 MHz, $CDCl_3$): δ ppm 4.87 (s, 4H, 2× CH_2-N), 6.91–6.89 (d, 2H, $J = 7.9$ Hz), 7.08–7.04 (m, 2H), 7.15–7.13 (d, 4H, $J = 7.6$ Hz), 7.24 (bs, 6H), 7.49 (s, 2H), 7.68–7.66 (d, 2H, $J = 7.6$ Hz). ^{13}C NMR (100 MHz, $CDCl_3$): δ ppm 52.55 (N-CH_2), 124.72, 125.27, 126.66, 129.12, 129.87, 134.40, 135.35, 136.85, 140.30, 159.68 (C=O). ESI-MS m/z [M + H] = 673.2.

*N^1,N^2-bis(3-iodophenyl)-N^1,N^2-bis(4-methylbenzyl)-oxamide (**2s**)*

Intermediate 3-iodo-*N*-(4-methylbenzyl)aniline was reacted with oxalyl chloride following the general procedure to give the product **2s** as a white solid with a yield of 90 %; mp 143–147 °C. ^{1}H NMR (400 MHz, $CDCl_3$): δ ppm 2.32 (s, 6H, 2× CH_3), 4.86 (s, 4H, 2× CH_2-N), 6.85–6.83 (d, 2H, $J = 8.0$ Hz), 7.03–7.00 (d, 4H, $J = 8.1$ Hz), 7.04–7.02 (d, 4H, $J = 8.1$ Hz), 7.28 (s, 2H), 7.32–7.31 (d, 2H, $J = 7.9$ Hz), 7.46–7.41 (m, 2H). ^{13}C NMR (100 MHz, $CDCl_3$): δ ppm 20.03 (Ph-CH_3), 50.53 (N-CH_2), 122.46, 126.64, 127.85, 128.56, 130.73, 135.84, 136.02, 138.21, 140.02, 160.15 (C=O). ESI-MS m/z [M + H] = 701.3.

A general procedure for the synthesis of fumaramide compounds (**3a**–**s**)

A mixture of meta-substituted benzaniline compound (1.3 mmol), TEA (1.3 mmol), and dry ethylacetate (5 mL). The mixture was cooled with an ice bath to 0–5 °C and fumaryl chloride (0.65 mmol) in 5 mL dry ethylacetate was added dropwise by syringe over 30 min. The reaction mixture was stirred at room temperature for over night. The

reaction mixture was quenched with 50 mL of distilled water and the aqueous phase was extracted with two portions of CH_2Cl_2. The combined organic layers were dried over $MgSO_4$, filtered and concentrated by rotary evaporation. The target compounds were recrystallized from ethanol.

*N^1,N^4-dibenzyl-N^1,N^4-di-m-tolyl-fumaramide (**3a**)*

Intermediate 3-methyl-*N*-(benzyl)aniline was reacted with fumaryl chloride following the general procedure to give the product **3a** as a white solid with a yield of 61 %; mp 180–184 °C. ^{1}H NMR (400 MHz, $CDCl_3$): δ ppm 2.31 (s, 6H, 2× CH_3), 4.88 (s, 4H, 2× CH_2-N), 6.75–6.74 (d, 2H, $J = 7.60$ Hz), 6.81 (s, 2H, fumaryl CH=CH), 6.89 (s, 2H), 7.13–7.11 (d, 4H, $J = 7.60$ Hz), 7.16–7.14 (m, 2H), 7.22–7.18 (m, 6H), 7.26–7.24 (d, 2H, $J = 7.6$ Hz). ^{13}C NMR (100 MHz, $CDCl_3$): δ ppm 21.29 (Ph-CH_3), 53.58 (CH_2-N), 125.28, 127.40 (CH=CH), 128.35, 128.49, 128.63, 129.04, 129.16, 132.07, 137.07, 139.75, 141.22, 164.43 (C=O). ESI-MS *m/z* [M + H] = 475.1.

*N^1,N^4-bis(4-methylbenzyl)-N^1,N^4-di-m-tolyl-fumaramide (**3b**)*

Intermediate 3-methyl-*N*-(4-methylbenzyl)aniline was reacted with fumaryl chloride following the general procedure to give the product **3b** as a white solid with a yield of 55 %; mp 202–204 °C. ^{1}H NMR (400 MHz, $CDCl_3$): δ ppm 2.29 (s, 6H), 2.32 (s, 6H), 4.83 (s, 4H, 2× CH_2-N), 6.74–6.72 (d, 2H, $J = 7.7$ Hz), 6.81 (s, 2H, ethylene protons CH=CH), 6.88 (s, 2H), 7.00 (bs, 8H), 7.12–7.10 (d, 2H, $J = 7.8$ Hz), 7.22–7.18 (m, 2H). ^{13}C NMR (100 MHz, $CDCl_3$): δ ppm 21.09 (*p*-CH_3), 21.29 (*m*-CH_3), 53.33 (CH_2-N), 125.33, 128.50 (CH=CH), 128.61, 129.01, 129.37, 132.07, 134.06, 137.00, 139.69, 141.30, 164.38 (C=O). ESI-MS *m/z* [M + H] = 503.1.

*N^1,N^4-dibenzyl-N^1,N^4-bis(3-(trifluoromethyl)phenyl)-fumaramide (**3c**)*

Intermediate 3-trifluoromethyl-*N*-(benzyl)aniline was reacted with fumaryl chloride following the general procedure to give the product **3c** as a white solid with a yield of 52 %; mp 161–165 °C. ^{1}H NMR (400 MHz, $CDCl_3$): δ ppm 4.92 (s, 4H, 2× CH_2-N), 6.83 (s, 2H, ethylene protons CH=CH), 7.12–7.10 (m, 6H), 7.26–7.24 (m, 2H), 7.29–7.26 (m, 6H), 7.50–7.48 (d, 2H, $J = 7.8$ Hz), 7.60 (s, 2H). ^{13}C NMR (100 MHz, $CDCl_3$): δ ppm 53.49 (CH_2-N), 124.87, 125.20 (CH=CH), 127.85, 128.63, 130.41, 131.82, 132.29, 136.20, 141.65, 163.94 (C=O). ESI-MS *m/z* [M + H] = 583.4.

*N^1,N^4-bis(4-methylbenzyl)-N^1,N^4-bis(3-(trifluoromethyl)phenyl)-fumaramide (**3d**)*

Intermediate 3-trifluoromethyl-*N*-(4-methylbenzyl)aniline was reacted with fumaryl chloride following the general procedure to give the product **3d** as a white solid with a yield of 46 %; mp 176–180 °C. ^{1}H NMR (400 MHz, $CDCl_3$): δ ppm 2.29 (s, 6H, 2× Ph-CH_3), 4.87 (s, 4H, 2× CH_2-N), 6.80 (s, 2H, ethylene protons CH=CH), 7.00–6.90 (d, 2H, $J = 7.9$ Hz), 7.05–7.03 (d, 4H, $J = 8.6$ Hz), 7.11–7.09 (d, 4H, $J = 7.8$ Hz), 7.27–7.26 (m, 2H), 7.49–7.47 (d, 2H, $J = 7.4$ Hz), 7.59 (s, 2H). ^{13}C NMR (100 MHz, $CDCl_3$): δ ppm 21.08 (Ph-CH_3), 53.25 (CH_2-N), 125.11, 128.62 (CH=CH), 129.26, 130.35, 131.88, 132.28, 133.17, 137.57, 141.72, 163.90 (C=O). ESI-MS *m/z* [M + H] = 611.2.

*N^1,N^4-dibenzyl-N^1,N^4-bis(3-ethylphenyl)-fumaramide (**3e**)*

Intermediate 3-ethyl-*N*-(benzyl)aniline was reacted with fumaryl chloride following the general procedure to give the product **3e** as a white solid with a yield of 16 %; mp 138–140 °C. ^{1}H NMR (400 MHz, $CDCl_3$): δ ppm 1.19–1.15 (t, 6H, 2× CH_2CH_3), 2.62–2.57 (q, 4H, 2× CH_2CH_3), 4.88 (s, 4H, 2× CH_2-N), 6.90 (s, 2H, ethylene protons CH=CH), 6.78–6.77 (d, 2H, $J = 7.9$ Hz), 7.15–7.13 (m, 6H), 7.24–7.22 (m, 6H), 7.26 (s, 2H). ^{13}C NMR (100 MHz, $CDCl_3$): δ ppm 15.21 (CH_2-CH_3), 28.53 (CH_2-CH_3), 53.50 (CH_2-N), 125.37, 127.39, 127.79, 128.34, 128.69, 129.49 (CH=CH), 132.12, 137.12, 141.24, 164.47 (C=O). ESI-MS *m/z* [M + H] = 503.8.

*N^1,N^4-bis(3-ethylphenyl)-N^1,N^4-bis(4-methylbenzyl)-fumaramide (**3f**)*

Intermediate 3-ethyl-*N*-(4-methylbenzyl)aniline was reacted with fumaryl chloride following the general procedure to give the product **3f** as a yellow solid with a yield of 50 %; mp 171–173 °C. ^{1}H NMR (400 MHz, $CDCl_3$): δ ppm 1.20–1.16 (t, 6H, 2× CH_2CH_3), 2.28 (s, 6H, 2× CH_3-Ph), 2.63–2.58 (q, 4H, 2× CH_2CH_3), 4.84 (s, 4H, 2× CH_2-N), 6.78–6.76 (bs, 4H), 6.88 (s, 2H, ethylene protons CH=CH), 7.03 (bs, 8H), 7.15–7.13 (d, 2H, $J = 7.69$ Hz), 7.26–7.21 (m, 2H). ^{13}C NMR (100 MHz, $CDCl_3$): δ ppm 15.21 (CH_2-CH_3), 21.08 (Ph-CH_3), 28.53 (CH_2-CH_3), 53.26 (CH_2-N), 125.43, 127.41, 127.72, 128.67, 129.00, 129.44 (CH=CH), 132.12, 134.11, 137.00, 141.32, 145.93, 164.42 (C=O). ESI-MS *m/z* [M + H] = 531.6.

*N^1,N^4-dibenzyl-N^1,N^4-bis(3-methoxyphenyl)-fumaramide (**3g**)*

Intermediate 3-methoxy-*N*-(benzyl)aniline was reacted with fumaryl chloride following the general procedure to

give the product **3g** as a white solid with a yield of 76 %; mp 180–182 °C. ^{1}H NMR (400 MHz, $CDCl_3$): δ ppm 2.31 (s, 6H, 2× OCH_3), 4.89 (s, 4H, 2× CH_2-N), 6.75–6.73 (d, 2H, $J = 7.60$ Hz), 6.81 (s, 2H, ethylene protons CH=CH), 6.90 (s, 2H), 7.13–7.11 (d, 4H, $J = 7.3$ Hz), 7.16–7.14 (m, 2H), 7.22–7.18 (m, 6H), 7.26–7.24 (d, 2H, $J = 7.6$ Hz). ^{13}C NMR (100 MHz, $CDCl_3$): δ ppm 21.09 (OCH_3), 53.57 (N-CH_2), 125.28, 127.39, 128.49, 128.63 (CH=CH), 129.05, 129.41, 132.07, 137.07, 139.74, 141.22, 164.43 (C=O). ESI-MS *m/z* [M + H] = 507.7.

*N^1,N^4-bis(3-methoxyphenyl)-N^1,N^4-bis(4-methylbenzyl)-fumaramide (**3h**)*

Intermediate 3-methoxy-*N*-(4-methylbenzyl)aniline was reacted with fumaryl chloride following the general procedure to give the product **3h** as a white solid with a yield of 37 %; mp 192–194 °C. ^{1}H NMR (400 MHz, $CDCl_3$): δ ppm 2.28 (s, 6H, 2× Ph-CH_3), 3.73 (s, 6H, 2× OCH_3), 4.84 (s, 4H, 2×CH_2-N), 6.45 (s, 2H, ethylene protons CH=CH), 6.56–6.54 (d, 2H, $J = 7.6$ Hz), 6.90 (s, 2H), 7.04 (bs, 8H), 7.23–7.21 (d, 2H, $J = 8.0$ Hz), 7.26–7.25 (m, 2H). ^{13}C NMR (100 MHz, $CDCl_3$): δ ppm 21.09 (Ph-CH_3), 53.18 (OCH_3), 55.33 (N-CH_2), 113.70, 113.93, 120.52, 128.66 (CH=CH), 130.30, 132.11, 134.03, 137.08, 142.42, 160.35, 164.32 (C=O). ESI-MS *m/z* [M + H] = 535.6.

*N^1,N^4-dibenzyl-N^1,N^4-bis(3-ethoxyphenyl)-fumaramide (**3i**)*

Intermediate 3-ethoxy-*N*-(benzyl)aniline was reacted with fumaryl chloride following the general procedure to give the product **3i** as a brown solid with a yield of 55 %; mp 184–188 °C. ^{1}H NMR (400 MHz, $CDCl_3$): δ ppm 1.39–1.36 (t, 6H, 2× CH_2CH_3), 3.93–3.91 (q, 4H, 2× CH_2CH_3), 4.88 (s, 4H, 2× CH_2-N), 6.50 (s, 2H, ethylene protons CH=CH), 6.55–6.53 (d, 2H, $J = 7.60$ Hz), 6.92 (s, 2H), 7.17–7.15 (d, 4H, $J = 7.6$ Hz), 7.19–7.16 (m, 2H), 7.23–7.21 (m, 6H), 7.26–7.24 (d, 2H, $J = 8.4$ Hz). ^{13}C NMR (100 MHz, $CDCl_3$): δ ppm 14.66 (OCH_2CH_3), 53.45 (OCH_2CH_3), 63.59 (N-CH_2), 114.34, 120.29, 127.43, 128.39 (CH=CH), 128.66, 130.31, 132.11, 137.08, 142.31, 159.77, 164.39 (C=O). ESI-MS *m/z* [M + H] = 536.8.

*N^1,N^4-bis(3-ethoxyphenyl)-N^1,N^4-bis(4-methylbenzyl)-fumaramide (**3j**)*

Intermediate 3-ethoxy-*N*-(4-methylbenzyl)aniline was reacted with fumaryl chloride following the general procedure to give the product **3j** as a white solid with a yield of 52 %; mp 178–182 °C. ^{1}H NMR (400 MHz, $CDCl_3$): δ ppm 1.40–1.37 (t, 6H, 2× OCH_2CH_3), 2.28 (s, 6H, 2× CH_3), 3.96–3.91 (q, 4H, 2× OCH_2CH_3), 4.83 (s, 4H, 2× CH_2-N), 6.50 (s, 2H), 6.54–6.52 (d, 2H, $J = 8.05$ Hz), 6.84–6.82 (d, 2H, $J = 8.4$ Hz), 6.90 (s, 2H, ethylene protons CH=CH), 7.06–7.04 (bs, 8H), 7.26–7.19 (m, 2H). ^{13}C NMR (100 MHz, $CDCl_3$): δ ppm 14.66 (OCH_2CH_3), 21.08 (Ph-CH_3), 53.19 (OCH_2CH_3), 63.59 (N-CH_2), 114.27, 114.36, 120.35, 128.64 (CH=CH), 129.04, 130.26, 132.11, 134.06, 137.03, 142.39, 159.74, 164.34 (C=O). ESI-MS *m/z* [M + H] = 563.1.

*N^1,N^4-dibenzyl-N^1,N^4-bis(3-fluorophenyl)-fumaramide (**3k**)*

Intermediate 3-fluoro-*N*-(benzyl)aniline was reacted with fumaryl chloride following the general procedure to give the product **3k** as a brown solid with a yield of 73 %; mp 162–165 °C. ^{1}H NMR (400 MHz, $CDCl_3$): δ ppm 4.90 (s, 4H, 2× CH_2-N), 6.73 (s, 2H, ethylene protons CH=CH), 6.78–6.76 (d, 2H, $J = 7.9$ Hz), 7.07–7.05 (m, 2H), 7.16–7.30 (d, 4H, $J = 7.4$ Hz), 7.30–7.25 (m, 6H), 7.33–7.30 (d, 2H, $J = 8.0$ Hz). ^{13}C NMR (100 MHz, $CDCl_3$): δ ppm 53.45 (N-CH_2), 115.56, 115.67, 124.11, 127.70 (CH=CH), 128.56, 130.85, 130.95, 132.18, 136.50, 142.66, 161.67, 164.07 (C=O). ESI-MS *m/z* [M + H] = 483.9.

*N^1,N^4-bis(3-fluorophenyl)-N^1,N^4-bis(4-methylbenzyl)-fumaramide (**3l**)*

Intermediate 3-fluoro-*N*-(4-methylbenzyl)aniline was reacted with fumaryl chloride following the general procedure to give the product **3l** as a brown solid with a yield of 34 %; mp 189–191 °C. ^{1}H NMR (400 MHz, $CDCl_3$): δ ppm 2.29 (s, 6H, 2× CH_3), 4.85 (s, 4H, 2× CH_2-N), 6.78–6.70 (m, 4H), 6.87 (s, 2H, ethylene protons CH=CH), 7.03–7.01 (d, 4H, $J = 8.3$ Hz), 7.06–7.04 (d, 4H, $J = 8.3$ Hz), 7.30–7.28 (d, 2H, $J = 8.0$ Hz), 7.34–7.32 (m, 2H). ^{13}C NMR (100 MHz, $CDCl_3$): δ ppm 21.11 (Ph-CH_3), 53.19 (N-CH_2), 115.38, 115.60, 124.15, 128.57 (CH=CH), 129.21, 130.80, 130.90, 132.18, 137.38, 142.73, 161.65, 164.13 (C=O). ESI-MS *m/z* [M + H] = 511.0.

*N^1,N^4-dibenzyl-N^1,N^4-bis(3-chlorophenyl)-fumaramide (**3m**)*

Intermediate 3-chloro-*N*-(benzyl)aniline was reacted with fumaryl chloride following the general procedure to give the product **3m** as a brown solid with a yield of 44 %; mp 178–180 °C. ^{1}H NMR (400 MHz, $CDCl_3$): δ ppm 4.89 (s, 4H, 2× CH_2-N), 6.84–6.83 (d, 2H, $J = 7.7$ Hz), 6.86 (s, 2H, ethylene protons CH=CH), 7.03 (s, 2H), 7.15–7.13 (d, 4H, $J = 8.1$ Hz), 7.25–7.24 (m, 2H), 7.29–7.26 (m, 6H), 7.34–7.32 (d, 2H, $J = 8.0$ Hz). ^{13}C NMR (100 MHz, $CDCl_3$): δ ppm 53.51 (N-CH_2), 126.68, 127.73, 128.21, 128.50 (CH=CH), 128.60, 128.70, 130.65, 132.20, 135.26, 136.42, 142.32, 164.04 (C=O). ESI-MS *m/z* [M + H] = 516.9.

*N^1,N^4-bis(3-chlorophenyl)-N^1,N^4-bis(4-methylbenzyl)-fumaramide (**3n**)*

Intermediate 3-chloro-*N*-(4-methylbenzyl)aniline was reacted with fumaryl chloride following the general procedure to give the product **3n** as a brown solid with a yield of 36 %; mp 197–199 °C. ^{1}H NMR (400 MHz, $CDCl_3$): δ ppm 2.29 (s, 6H, 2× CH_3), 4.84 (s, 4H, 2× CH_2-N), 6.81 (s, 2H, ethylene protons CH=CH), 6.84 (s, 2H), 7.02 (bs, 8H), 7.06–7.04 (d, 2H, $J = 8.2$ Hz), 7.28–7.24 (m, 2H), 7.32–7.30 (d, 2H, $J = 8.0$ Hz). ^{13}C NMR (100 MHz, $CDCl_3$): δ ppm 21.11 (Ph-CH_3), 53.19 (N-CH_2), 115.38, 115.60, 124.15, 128.57 (CH=CH), 128.69, 129.21, 130.80, 130.90, 132.18, 137.38, 142.73, 164.13 (C=O). ESI-MS *m/z* [M + H] = 544.5.

*N^1,N^4-dibenzyl-N^1,N^4-bis(3-bromophenyl)-fumaramide (**3o**)*

Intermediate 3-bromo-*N*-(benzyl)aniline was reacted with fumaryl chloride following the general procedure to give the product **3o** as a brown solid with a yield of 56 %; mp 174–178 °C. ^{1}H NMR (400 MHz, $CDCl_3$): δ ppm 4.88 (s, 4H, 2× CH_2-N); 6.85 (s, 2H, ethylene protons CH=CH); 6.88 (bs, 2H); 7.14 (m, 4H); 7.21–7.20 (m, 4H, Ha); 7.24 (bs, 6H); 7.48–7.46 (d, 2H, $J = 7.8$ Hz). ^{13}C NMR (100 MHz, $CDCl_3$): δ ppm 53.54 (N-CH_2), 123.10, 127.20, 127.74, 128.50, 128.63 (CH=CH), 130.91, 131.06, 131.61, 132.20, 136.40, 142.42, 164.02 (C=O). ESI-MS *m/z* [M + H] = 605.5

*N^1,N^4-bis(3-bromophenyl)-N^1,N^4-bis(4-methylbenzyl)-fumaramide (**3p**)*

Intermediate 3-bromo-*N*-(4-methylbenzyl)aniline was reacted with fumaryl chloride following the general procedure to give the product **3p** as a white solid with a yield of 59 %; mp 196–198 °C. ^{1}H NMR (400 MHz, $CDCl_3$): δ ppm 2.29 (s, 6H, 2× CH_3), 4.84 (s, 4H, 2× CH_2-N), 6.83 (s, 2H, ethylene protons CH=CH), 6.87–6.85 (d, 2H, $J = 8.0$ Hz), 7.03–7.00 (d, 4H, $J = 8.0$ Hz), 7.06–7.00 (d, 4H, $J = 8.0$ Hz), 7.18 (s, 2H), 7.22–7.20 (d, 2H, $J = 8.0$ Hz), 7.48–7.46 (m, 2H). ^{13}C NMR (100 MHz, $CDCl_3$): δ ppm 21.10 (Ph-CH_3), 53.29 (N-CH_2), 123.05, 127.24, 128.61, 129.21 (CH=CH), 130.85, 131.06, 131.52, 132.21, 133.37, 137.40, 142.51, 163.98 (C=O). ESI-MS *m/z* [M + H] = 634.3.

*N^1,N^4-dibenzyl-N^1,N^4-bis(3-iodophenyl)-fumaramide (**3r**)*

Intermediate 3-iodo-*N*-(benzyl)aniline was reacted with fumaryl chloride following the general procedure to give the product **3r** as a white solid with a yield of 50 %; mp 210–212 °C. ^{1}H NMR (400 MHz, $CDCl_3$): δ ppm 4.87 (s, 4H, 2× CH_2-N), 6.84 (s, 2H, ethylene protons CH=CH), 6.91–6.89 (d, 2H, $J = 7.6$ Hz), 7.08–7.04 (m, 2H), 7.15–7.13 (d, 4H, $J = 7.3$ Hz), 7.24 (bs, 6H), 7.49 (s, 2H), 7.68–7.66 (d, 2H, $J = 7.8$ Hz). ^{13}C NMR (100 MHz, $CDCl_3$): 53.55 (N-CH_2), 127.72, 127.89, 128.55 (CH=CH), 128.66, 131.03, 132.21, 136.40, 136.84, 137.49, 142.30, 164.01 (C=O). ESI-MS *m/z* [M + H] = 699.7.

*N^1,N^4-bis(3-iodophenyl)-N^1,N^4-bis(4-methylbenzyl)-fumaramide (**3s**)*

Intermediate 3-iodo-*N*-(4-methylbenzyl)aniline was reacted with fumaryl chloride following the general procedure to give the product **3s** as a white solid with a yield of 39 %; mp 142–147 °C. ^{1}H NMR (400 MHz, $CDCl_3$): δ ppm 2.30 (s, 6H, 2× CH_3), 4.60 (s, 4H, 2× CH_2-N), 6.66 (s, 2H, ethylene protons CH=CH), 6.97–6.95 (d, 2H, $J = 7.9$ Hz), 7.05–7.01 (bs, 8H,), 7.08 (s, 2H); 7.13–7.12 (m, 2H); 7.69–7.67 (d, 2H). ^{13}C NMR (100 MHz, $CDCl_3$): 21.15 (Ph-CH_3), 51.58 (N-CH_2), 128.20, 128.30, 129.26 (CH=CH), 129.45, 130.41, 132.73, 137.11, 137.37, 137.54, 140.35, 163.85 (C=O). ESI-MS *m/z* [M + H] = 727.5.

Inhibition studies on AChE and BuChE

AChE (E.C. 3.1.1.7, from electric eel), BuChE (E.C. 3.1.1.8, from equine serum), 5,5-dithiobis-(2-nitrobenzoic acid) DTNB, acetylthiocholine iodide (ATCI), and butyrylthiocholine iodide (BTCI) were purchased from Sigma Aldrich. Inhibitory activities of AChE and BuChE of the test compounds were evaluated by colorimetric Ellman's method (Ellman *et al*., 1961) with some modifications using commercially available neostigmine bromide (Skrzypek *et al*., 2013), galantamine bromide (Singh *et al*., 2013), and ambenonium dichloride (Musileka *et al*., 2011) as the reference compounds. The test compounds were dissolved in dimethylsulphoxide and then diluted in 50 mM Tris buffer (pH 8.0) to provide a final concentration range. In a 96-well plate, the assay medium in each well consisted of 50 µL of a Tris buffer, 125 µL of 3 mM DTNB (Ellman's reagent), 25 µL of 0.2 U/mL enzyme (AChE or BuChE) and 15 mM substrate (ATCI or BTCI). The assay mixture containing enzyme, buffer, DTNB and 25 µL of inhibitor compound was preincubated for 15 min at 37 °C, before the substrate was added to begin the reaction. Galantamine bromide, neostigmine bromide, ambenonium dichloride, and all test compounds were prepared at different concentrations such as 0.195, 0.39, 0.78, 1.56, 3.13, 6.25, 12.5, 25, 50, and 100 µg/mL. The absorbance of the reaction mixture was then measured

three times at 412 nm every 45 s using a microplate reader (Bio-Tek ELx800, USA). Results are presented as means ± standard errors of the experiment. The IC_{50} values of the compounds showing percentage inhibition, the measurements and calculations were evaluated by nonlinear regression analysis using GraphPad Prism software.

Kinetic study

Compounds **3o**, **3p**, and **2h** were selected for kinetic measurements because they were found to have the highest inhibitory activity against AChE and BuChE, respectively. The test was carried out without the inhibitor and in 0.02, 0.03, and 0.04 μM concentrations of the inhibitors **3o** and **3p**, 0.01, 0.02, and 0.03 μM concentrations for the inhibitor **2h**. Substrate concentrations were varied from 0.1 to 1.5 mM. The obtained data were used to create substrate-velocity curves, which were transformed in GraphPad Prism to Lineweaver–Burk plots.

Spectrophotometric measurement of complex with Cu^{2+} and Fe^{2+}

The study of metal chelation was performed in ethanol at room temperature using UV–Vis spectrophotometer (Thermo Electron Heλios) with wavelength ranging from 200 to 500 nm. The UV absorption of the test compounds **3o** and **2h**, in the absence or presence of with $CuSO_4$ and $FeSO_4$, was recorded in a 1 cm quartz cuvette after 20 min at room temperature. The final volume of reaction mixture was 3 mL, and final concentrations of the test compounds and metals were 100 μM. All reaction mixtures were repeated for at least three times.

Molecular modeling

The docking study was performed using Surflex-Dock in Sybyl-X 2.0 by Tripos Associates. 3D structures of the compounds **2h**, **3o**, and **3p** were constructed using the Sybyl sketcher module. The structures were minimized using the steepest descent conjugated gradient method until the gradient was 0.001 kcal/mol, max iterations: 5000 with the Tripos force field with the Gasteiger Huckel charge. The simulation system was built on the crystal structures of 1ACJ and 1P0I which were obtained from the Protein Data Bank. At the commencement of docking, all the water and ligands were removed and the random hydrogen atoms were added. Docking calculations using Surflex-Dock for 1ACJ and 1P0I were performed through protomol generation by ligand. The parameters used were threshold 0.5 and bloat 0.

Result and discussion

Chemistry

In the first step, starting benzanilines (**1a**–**s**) were prepared using a microwave heating method under solvent-free, phase-transfer catalysis conditions. N^1,N^2-diaryl-N^1,N^2-bis-(3-substituted-phenyl)-oxamides (**2a**–**s**) were synthesized by the reaction of oxalyl chloride with meta-substituted benzanilines as key intermediates in tetrahydrofuran in the presence of TEA with moderate to good yields (40–90 %). The other target compounds, N^1,N^4-diaryl-N^1,N^4-bis-(3-substituted-phenyl)-fumaramides (**3a**–**s**), were obtained in moderate yields (16–76 %) by following the same procedure described in the previously reported literature (Yerdelen, 2012). The obtained spectroscopic data are in accordance with the predicted structures. The synthesis scheme of the compounds is presented in Scheme 1. In the proton nuclear magnetic resonance (^{1}H-NMR) spectra, the resonance signals of ethylene bridge protons are usually registered as singlets in the range of 6.45–6.90 ppm and signals for aromatic protons showed between δ 6.51 and 7.68 ppm. The N-CH_2 protons appeared at δ 4.80–4.92 ppm. The carbon nuclear magnetic resonance (^{13}C-NMR) spectrum shows characteristic carbon resonance frequencies of carbonyl atoms in the range of 157.20–161.23 ppm for the compounds **2a**–**s** and 164.47–163.85 ppm for the compounds **3a**–**s**. The aromatic carbons appeared at δ 113.70–161.67 ppm and N-CH_2 groups appeared at δ 51.58–63.59 ppm. In the positive electron impact (EI) mass spectra, the molecular ion peaks [M + H] show that the predicted compound has formed.

Cholinesterase inhibitory activity

The inhibitory activity of the compounds **2a**–**s** and **3a**–**s** against AChE (from electric eel) and BuChE (from equine serum) was measured according to the colorimetric assay of Ellman *et al*. (1961). Neostigmine, ambenonium, and galantamine were used as the reference compounds. The IC_{50} values of all tested compounds and their selectivity index for AChE over BuChE are summarized in Table 1. As seen in Table 1, all new fumaramide compounds **3a**–**s** showed good inhibitory activity to both ChEs with micromolar concentrations. Among the target compounds, **3o** (IC_{50} = 0.03 μM) showed the most potent inhibitory activity for AChE, being 2.33-, 35-, and 63-fold stronger than the reference compounds neostigmine (IC_{50} = 0.07 μM), galantamine (IC_{50} = 1.05 μM), and ambenonium (IC_{50} = 1.89 μM), respectively. In contrast, **3p** exhibited the strongest inhibition to BuChE with an IC_{50} value of 0.03 μM, which was 3-, 154-, and 441-fold more

Table 1 In vitro inhibition IC_{50} (μM) and selectivity of target compounds **2a–s** and **3a–s** on AChE and BuChE

Compound	R1	R2	IC_{50} (μM)		Selectivity index[c]	Log *P**
			AChE[a]	BuChE[b]		
2a	CH_3	H	>100	0.51 ± 0.1	0.005	6.88
2b	CH_3	CH_3	>100	42.78 ± 1.7	0.20	7.85
2c	CF_3	H	>100	>100	–	7.75
2d	CF_3	CH_3	>100	>100	–	8.72
2e	C_2H_5	H	>100	>100	–	7.72
2f	C_2H_5	CH_3	>100	>100	–	8.69
2g	OCH_3	H	>100	87.22 ± 1.1	0.87	5.65
2h	OCH_3	CH_3	>100	0.02 ± 0.31	0.0002	6.63
2i	OC_2H_5	H	>100	>100	–	6.33
2j	OC_2H_5	CH_3	>100	>100	–	7.30
2k	F	H	>100	>100	–	6.22
2l	F	CH_3	>100	>100	–	7.20
2m	Cl	H	>100	>100	–	7.02
2n	Cl	CH_3	>100	>100	–	8.00
2o	Br	H	>100	>100	–	7.56
2p	Br	CH_3	>100	>100	–	8.54
2r	I	H	>100	>100	–	8.62
2s	I	CH_3	>100	>100	–	9.60
3a	CH_3	H	42.19 ± 3.9	60.81 ± 7.5	1.44	7.05
3b	CH_3	CH_3	>100	6.59 ± 2.1	0.066	8.02
3c	CF_3	H	30.01 ± 5.9	0.21 ± 0.7	0.007	7.92
3d	CF_3	CH_3	81.89 ± 2.9	22.26 ± 1.5	0.27	8.89
3e	C_2H_5	H	77.45 ± 1.8	>100	1.29	7.88
3f	C_2H_5	CH_3	2.15 ± 6.5	>100	46.51	8.86
3g	OCH_3	H	0.2 ± 0.1	2.79 ± 0.3	13.95	5.82
3h	OCH_3	CH_3	47.62 ± 0.7	0.32 ± 2.5	0.007	6.80
3i	OC_2H_5	H	>100	0.05 ± 5.4	0.0005	6.50
3j	OC_2H_5	CH_3	15.72 ± 0.6	0.27 ± 1.7	0.017	7.47
3k	F	H	24.18 ± 31.5	0.04 ± 2.8	0.0016	6.39
3l	F	CH_3	0.14 ± 0.2	18.7 ± 0.4	133.57	7.36
3m	Cl	H	35.42 ± 3.6	0.08 ± 4.6	0.002	7.19
3n	Cl	CH_3	0.57 ± 4.4	7.21 ± 1.8	12.64	8.16
3o	Br	H	0.03 ± 0.9	0.56 ± 0.4	18.70	7.73
3p	Br	CH_3	0.24 ± 1.7	0.03 ± 0.9	0.13	8.71
3r	I	H	0.53 ± 0.5	3.52 ± 8.5	6.64	8.79
3s	I	CH_3	0.95 ± 6.8	1.06 ± 1.2	1.12	9.76
Galantamine			1.05 ± 0.45	13.22 ± 0.46	12.6	
Neostigmin			0.07 ± 0.01	0.09 ± 0.002	1.29	
Ambenonium			1.89 ± 0.001	4.61 ± 0.005	2.43	

* Logarithm of the partition coefficient (Log *P*) values were calculated using ChemDraw Ultra ver. 7.0 (CambridgeSoft, USA)

[a] 50 % inhibitory concentration (mean ± SD of three experiments) of AChE

[b] 50 % inhibitory concentration (mean ± SD of three experiments) of BuChE

[c] Selectivity for AChE = IC_{50} (BuChE)/IC_{50} (AChE)

potent than those of neostigmine (IC_{50} = 0.09 μM), ambenonium (IC_{50} = 4.61 μM), and galantamine (IC_{50} = 13.22 μM).

The oxamide derivatives (**2a–s**) did not exhibit inhibitory activity against AChE (Table 1). Compounds **2b** and **2g** were found to have a moderate inhibitory activity on

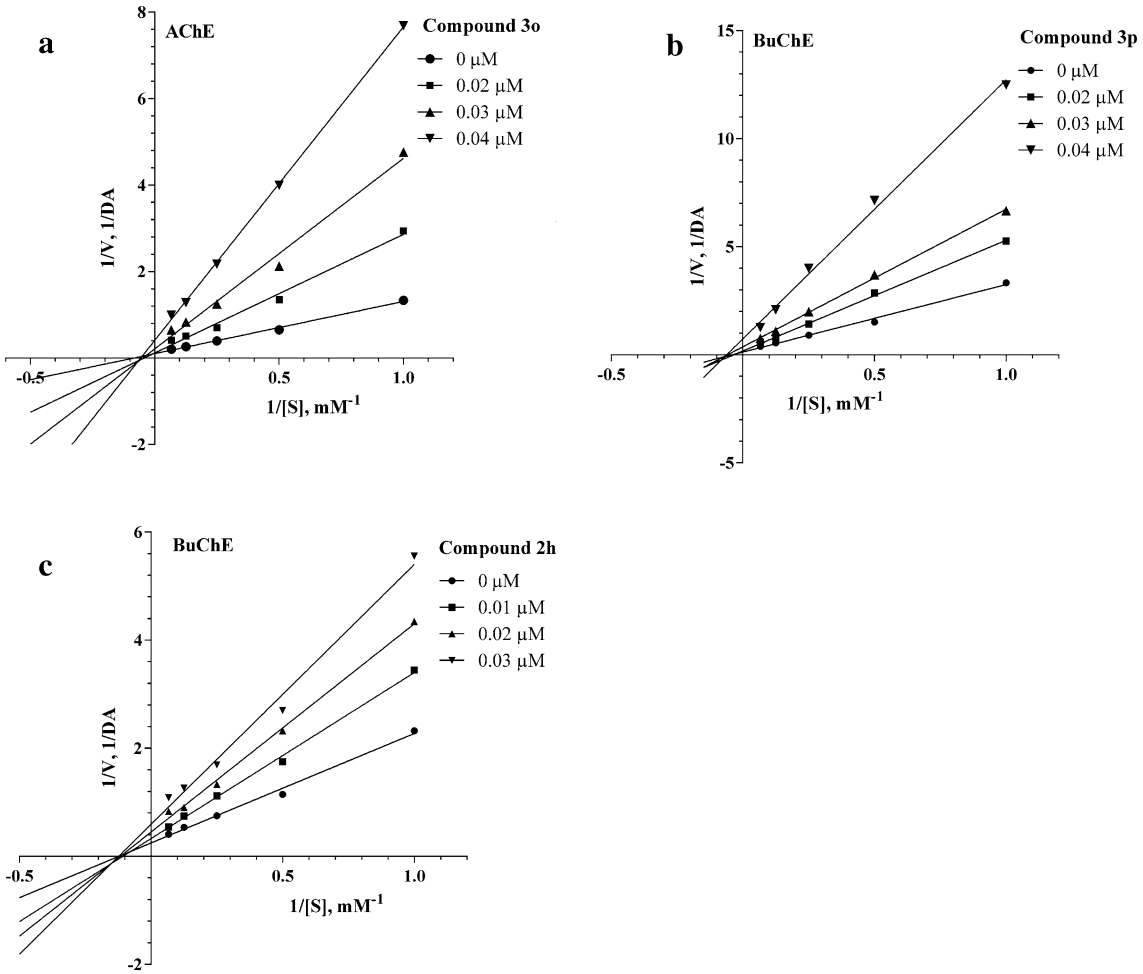

Fig. 1 The Lineweaver–Burk plots for the inhibition of cholinesterase enzymes by compounds **3o** (**a**), **3p** (**b**), and **2h** (**c**)

BuChE, with an IC_{50} of 42.78 and 87.22 μM, respectively. Compounds **2a** and **2h** exhibited the strongest inhibition to BuChE with IC_{50} values of 0.51 and 0.02 μM, respectively. The other compounds in the series were considered to be inactive, since their IC_{50} values were more than 100 μM.

The target compounds (**2a–s** and **3a–s**) were synthesized using different meta-substituted anilines with varying electronic properties. In general, the target compounds **3k–s** were found the most effective inhibitors against AChE and BuChE, which have various electron-drawing halogen groups (F, Cl, Br, I) at the meta-position of the phenyl ring. To support this approach, as shown in Table 1, **3a–b** possessing an electron-donating group ($–CH_3$) at the meta-position of the aniline ring moiety showed a decreased AChE inhibitory activity, while the corresponding compounds **3c–d** possessing an electron-drawing group ($–CF_3$) showed an increased AChE inhibitory activity. However compounds **3b** ($–CH_3$) and **3i** ($–OC_2H_5$), which have electron-donating groups at the meta-position, were the most inactive in the series for AChE inhibition. In addition, **3e** and **3f**, possessing an electron-donating group ($–C_2H_5$) at the meta-position, showed the most decreased BuChE inhibitory activity. These results imply that an electron-drawing group at the meta-position of the aniline ring is beneficial to AChE and BuChE inhibitory activity. By contrast, especially in the series **2a–s**, electron-donating groups showed an increase in both ChEs inhibition. It was also observed that within both series of meta-halogenated compounds cholinesterase inhibition activity increases with increasing electron-withdrawing effect.

The other physicochemical parameter, lipophilicity, is a property used in drug designing and drug discovery that has a major effect on absorption, distribution, metabolism, excretion and toxicity properties as well as pharmacological activity. The blood–brain barrier (BBB) represents a major obstacle to the delivery of drugs to the CNS. Particularly, CNS drugs cross BBB via the passive transport, which strongly depends on their lipophilicity.

From the IC_{50} values, the fumaramide derivatives seemed to be more effective than the oxamide derivatives **2a–s** on AChE inhibition due to the ethylene bridge for the linker between the two carbonyl groups in the **3a–s** series.

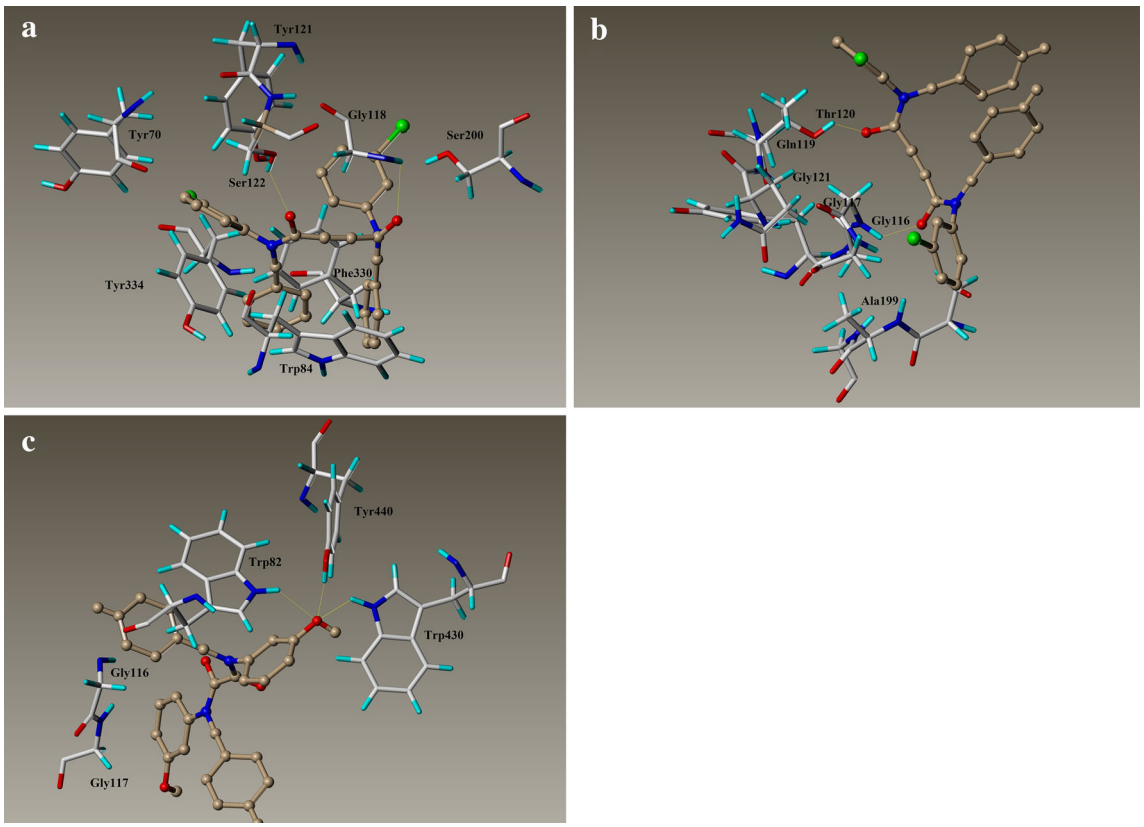

Fig. 2 Docking models of compound–enzyme complex. Compound **3o** (**a**) interacts with residues in the binding sites of TcAChE (**a**). Compounds **3p** (**b**) and **2h** (**c**) interacts with HuBuChE

A similar situation was seen with BuChE inhibition, (except for **2a** and **2h**). It can be stated that compounds in series **3a–s** with higher lipophilicity exhibited higher cholinesterase inhibition than the series **2a–s**. And these findings suggest us the anticholinesterase activity is strongly dependent on the presence of ethylene moiety in the inhibitors. In our previously reported study, the results of anticholinesterase activity showed that α,β-unsaturated moiety contributed to the interaction with cholinesterase enzymes (Yerdelen and Gul, 2013). The results of this study confirmed this approach.

Kinetic study

For the kinetic studies, the potent AChE inhibitor **3o** and BuChE inhibitors **3p** and **2h** were chosen. The mechanism of cholinesterase inhibition was investigated with Ellman's test (Ellman *et al*., 1961). The type of inhibition was illuminated from the analysis of Lineweaver–Burk plots, which were reciprocal rates versus reciprocal substrate concentrations for the different inhibitor concentrations resulting from the substrate-velocity curves for ChE. The plots showed that for AChE both increased slopes and intercepts at increasing concentration of the inhibitor **3o**, indicating a mixed-type inhibition (Fig. 1a). Thus, compound **3o** can bind to the CAS and the PAS of AChE. In Fig. 1b and c, the lines crossed the *x* axis in the same point (unchanged K_m) and decreased V_{max} with increasing inhibitor concentrations. This is a typical trend of non-competitive inhibition. Docking simulations showed that compounds **3p** and **2h** bound mainly to the CAS and PAS of BuChE, respectively.

Molecular modeling studies

Molecular modeling studies were performed to investigate possible interactions between the most active compounds, **3o** with AChE, and **3p** and **2h** with BuChE. The molecular modeling was performed with the docking program SYBYL X 2.0 (Surflex-Dock software). The structures of the enzymes were obtained from the Protein Data Bank. The docking results showed that the compound **3o** displayed multiple binding patterns with Torpedo californica (TcAChE-1ACJ), as shown in Fig. 2a. In the 1ACJ-**3o** complex, oxygen atom from the carbonyl group created a hydrogen bond with OH of Ser122 (2.0 Å) of PAS. And the oxygen atom of the other carbonyl group formed an interaction: H-bond with NH group of Gly118 (2.5 Å) at

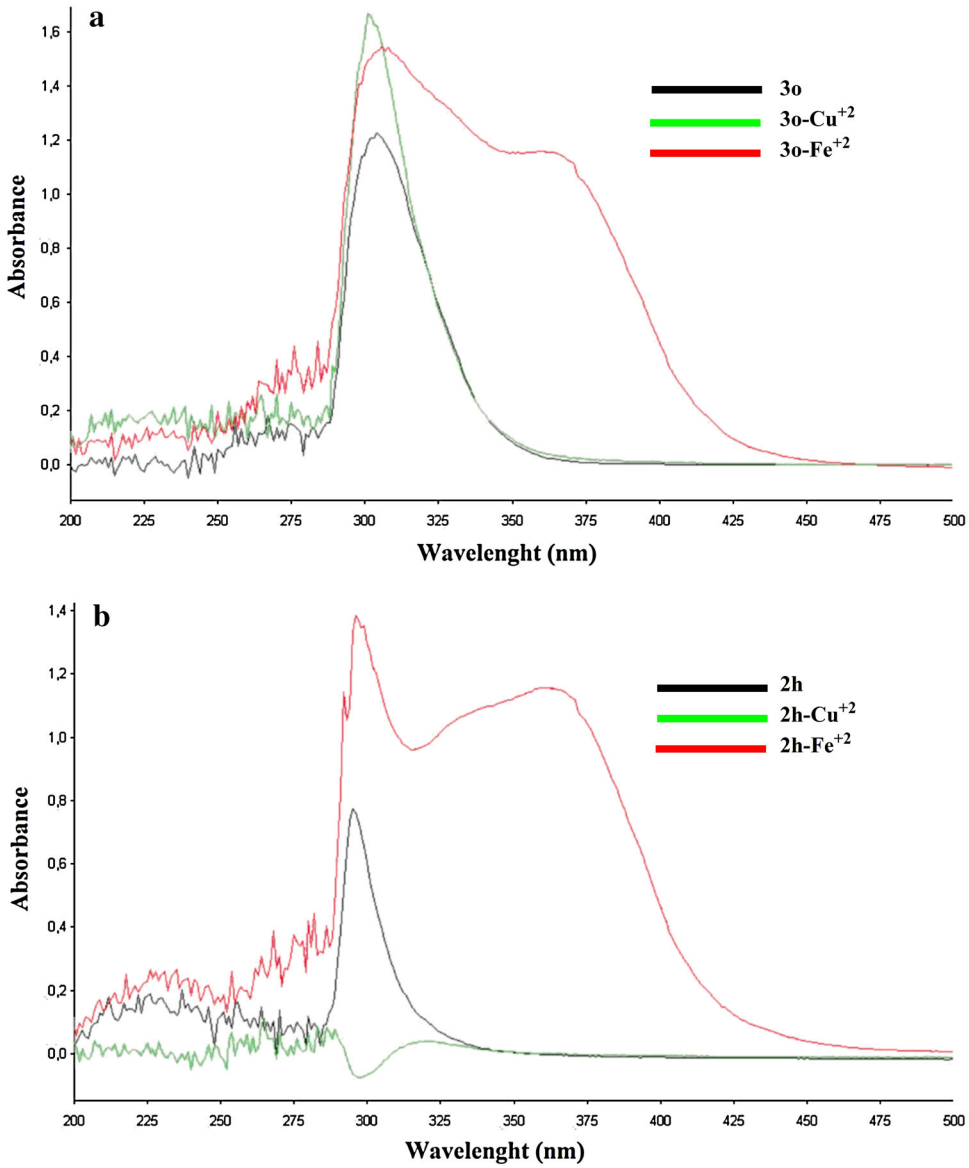

Fig. 3 UV–Vis (200–500 nm) absorption spectra of compound **3o** (**a**) and **2h** (**b**) alone or in the presence of $CuSO_4$ and $FeSO_4$. The final concentration of the compounds and metals were 100 μM

the CAS of the enzyme. The results indicate that the binding of **3o** to the CAS and PAS gorges of TcAChE explains the promising potency for AChE inhibition and reveals a mixed-type inhibition of the compound.

The most potent BuChE inhibitor, **3p**, showed interactions with Thr120 and Gly116 residues of human butyryl cholinesterase enzyme (HuBuChE-1P0I) (Fig. 2b). Hydrogen bond interactions between the carbonyl group and OH group of Thr120 (2.7 Å) at the CAS of HuBuChE was occured. In HuBuChE, the oxyanion hole consists of highly conserved N–H dipoles, derived from amino acids of the main chain: Gly116, Gly117, and Ala119. And the other carbonyl group showed an hydrogen bond interaction with NH group of Gly116 (1.9 Å). We also performed a docking simulation between **2h** and HuBuChE (1P0I) using same program. As shown in Fig. 2c, the 3-OCH_3 phenyl ring entered the PAS of BuChE and interacted with three hydrogen bonds with residues OH group of Tyr440 (1.9 Å), NH group of Trp82 (2.4 Å), and NH group of Trp430 (2.6 Å). The results of the interaction displayed non-competitive inhibition by the compounds **3p** and **2h**.

Metal chelating effect

The chelating effect of the most potent compounds, **3o** and **2h**, for the metals such as Cu^{2+} and Fe^{2+} in ethanol was studied by using UV–Visible spectrophotometry with wavelength ranging from 200 to 500 nm (Huang *et al.*, 2010; Joseph *et al.*, 2008). The UV absorption of the compounds **3o** and **2h** in ethanol changed with the titration of Cu^{2+} and Fe^{2+}. An increase in absorbance can be observed after adding $CuSO_4$ (shown in Fig. 3a), indicating the formation of

complex **3o**–Cu^{2+}. Similar behavior was also observed for the compound **3o** when using Fe^{2+}. These observations indicate that **3o** could effectively chelate Cu^{2+}, Fe^{2+}, and, thereby, could serve as a metal chelator in treating AD. Besides this, an increasing absorbance was obtained with the titration of Fe^{2+} and **2h**. This result indicates the formation of **2h**–Fe^{2+} metal complex. The absorbance intensity decreased with the titration of **2h**–Cu^{2+}, as shown Fig. 3b.

Conclusion

In summary, a series of new oxamide and fumaramide analogs was synthesized and evaluated as AChE and BuChE inhibitors. According to the inhibition data, the fumaramides generally showed moderate to high anticholinesterase activity in which compounds **3o** and **3p** were the most potent inhibitors acting in low micromolar concentrations toward AChE and HuBuChE, respectively. Compound **3o** ($IC_{50} = 0.03$ μM) was found the most potent AChE inhibitor in its series. Compound **3o** also showed strong affinity ($IC_{50} = 0.56$ μM) for BuChE but **3p** was found the most effective compound ($IC_{50} = 0.03$ μM) in the series. In series **2a**–**s**, only four compounds (**2a**, **2b**, **2g**, and **2h**) showed inhibitory activity exclusively for HuBuChE. Compound **2h** showed promising inhibitory ability ($IC_{50} = 0.02$ μM) toward HuBuChE better to standards galantamine, neostigmine, and ambenonium with high selectivity. The kinetic studies suggested that the inhibition mechanisms of the investigated compounds could be different. The docking simulation showed that modeled derivative **3o** created many interactions with the PAS and CAS gorges of TcAChE, confirming its high inhibitor potency and revealing a mixed-type inhibition. In addition, kinetic studies indicated that compounds **2h** and **3p** exhibited non-competitive inhibition against the HuBuChE enzyme. Consequently, the findings imply that the presence of an ethylene bridge in the fumaramide inhibitors had more influence than the oxamide derivatives on their inhibition of AChE and BuChE.

Acknowledgments This research work was supported by Ataturk University Research Fund (Project No: 2013/56), Turkey.

Conflict of interest The authors have declared no conflicts of interest with the presented data from this article.

References

Akasofu S, Kimura M, Kosasa I, Sawada K, Ogura H (2008) Study of neuroprotection of donepezil, a therapy for Alzheimer's disease. Chem Biol Interact 175:222–226

Basiri A, Murugaiyaha V, Osman H, Kumar RS, Kia Y, Awang KB, Ali MA (2013) An expedient, ionic liquid mediated multi-component synthesis of novel piperidone grafted cholinesterase enzymes inhibitors and their molecular modeling study. Eur J Med Chem 67:221–229

Brookmeyer R, Johnson E, Ziegler-Graham K, Arrighi HM (2007) Forecasting the global burden of Alzheimer's disease. Alzheimers Dement 3:186–191

Bullock R, Lane R (2007) Executive dyscontrol in dementia, with emphasis on subcortical pathology and the role of butyrylcholinesterase. Curr Alzheimer Res 4:277–293

Bush AI (2008) Drug development based on the metals hypothesis of Alzheimer's disease. J Alzheimer's Dis 15:223–240

Darvesh S, Hopkins DA, Geula C (2003) Neurobiology of butyrylcholinesterase. Nat Rev Neurosci 4:131–138

Dong J, Atwood CS, Anderson VE, Siedlak SL, Smith MA, Perry G, Carey PR (2003) Metal binding and oxidation of amyloid-beta within isolated senile plaque cores: Raman microscopic evidence. Biochemistry 42:2768–2773

Dumas JA, Newhouse PA (2011) The cholinergic hypothesis of cognitive aging revisited again: cholinergic functional compensation. Pharmacol Biochem Behav 99:254–261

Ellman GL, Courtney D, Andies V, Featherstone RM (1961) A new and rapid colorimetric determination of acetylcholinesterase activity. Biochem Pharmacol 7:88–95

Greig NH, Utsuki T, Ingram DK, Wang Y, Pepeu G, Scali C, Yu QS, Mamczarz J, Holloway HW, Giordano T, Chen D, Furukawa K, Sambamurti K, Brossi A, Lahiri DK (2005) Selective butyrylcholinesterase inhibition elevates brain acetylcholine, augments learning and lowers Alzheimer beta-amyloid peptide in rodent. Proc Natl Acad Sci 102:17213–17218

Hasan A, Khan KM, Sher M, Maharvi GM, Nawaz SA, Choudhary MI, Rahman AU, Supuran CT (2005) Synthesis and inhibitory potential towards acetylcholinesterase, butyrylcholinesterase and lipoxygenase of some variably substituted chalcones. J Enzyme Inhib Med Chem 20:41–47

Huang X, Moir RD, Tanzi RE, Bush AI, Rogers JT (2004) Redox-active metals, oxidative stress, and Alzheimer's disease pathology. Ann N Y Acad Sci 1012:153–163

Huang W, Lv D, Yu H, Sheng R, Kim SC, Wu P, Luo K, Li J, Hu Y (2010) Dual-target-directed 1,3-diphenylurea derivatives: BACE 1 inhibitor and metal chelator against Alzheimer's disease. Bioorg Med Chem 18:5610–5615

Jhee SS, Shiovitz T, Hartman RD, Messina J, Anand R, Sramek J, Cutler NR (2002) Centrally acting antiemetics mitigate nausea and vomiting in patients with Alzheimer's disease who receive rivastigmine. Clin Neuropharmacol 25:122–123

Joseph R, Ramanujam B, Acharya A, Khutia A, Rao CP (2008) Experimental and computational studies of selective recognition of Hg^{2+} by amide linked lower rim 1,3-dibenzimidazole derivative of calix[4]arene: species characterization in solution and that in the isolated complex, including the delineation of the nanostructures. J Org Chem 73:5745–5758

Kamal MA, Qu X, Yu QS, Tweedie D, Holloway HW, Li Y, Tan Y, Greig NH (2008) Tetrahydrofurobenzofuran cymserine, a potent butyrylcholinesterase inhibitor and experimental Alzheimer drug candidate, enzyme kinetic analysis. J Neural Transm 115: 889–898

Khoobi M, Alipour M, Moradi A, Sakhteman A, Nadri H, Razavi SF, Ghandi M, Foroumadi A, Shafiee A (2013) Design, synthesis, docking study and biological evaluation of some novel tetrahydrochromeno [3′,4′:5,6]pyrano[2,3-b]quinolin-6(7H)-one derivatives against acetyl- and butyrylcholinesterase. Eur J Med Chem 68:291–300

Lambert J, Heath S, Even G, Campion D, Sleegers K, Hiltunen M, Sleegers K, Hiltunen M (2009) Genome-wide association study identifies variants at CLU and CR1 associated with Alzheimer's disease. Nat Genet 41:1094–1099

Liu G, Huang W, Moir RD, Vanderburg CR, Lai B, Peng Z, Tanzi RE, Rogers JT, Huang X (2006) Metal exposure and Alzheimer's pathogenesis. J Struct Biol 155:45–51

Mesulam MM, Guillozet A, Show P, Levey A, Duysen EGM, Lockridge O (2002) Acetylcholinesterase knockouts establish central cholinergic pathways and can use butyrylcholinesterase to hydrolyze acetylcholine. Neuroscience 110:627–639

Musileka K, Komloova M, Holas O, Hrabinova M, Pohanka M, Dohnal V, Nachone F, Dolezal M, Kucaa K (2011) Preparation and in vitro screening of symmetrical bis-isoquinolinium cholinesterase inhibitors bearing various connecting linkage e Implications for early Myasthenia gravis treatment. Eur J Med Chem 46:811–818

Naj AC, Jun G, Beecham GW, Wang LS, Vardarajan BN, Buros J, Gallins PJ, Buxbaum JD, Jarvik GP, Crane PK, Larson EB, Bird TD, Boeve BF, Graff-Radford NR, De Jager PL, Evans D, Schneider JA (2011) Common variants at MS4A4/MS4A6E, CD2AP, CD33 and EPHA1 are associated with late-onset Alzheimer's disease. Nat Genet 43:436–441

Opazo C, Huang X, Cherny RA, Moir RD, Roher AE, White AR, Cappai R, Masters CL, Tanzi RE, Inestrosa NC, Bush AI (2002) Cu-dependent catalytic conversion of dopamine, cholesterol, and biological reducing agents to neurotoxic H_2O_2. J Biol Chem 277:40302–40308

Piazzi L, Rampa A, Bisi A, Gobbi S, Belluti F, Cavalli A, Bartolini M, Andrisano V, Valenti P, Recanatini M (2003) Extensive SAR and computational studies of 3-{4-[(benzylmethylamino)methyl]phenyl}-6,7-dimethoxy-2H-2-chromenone (AP2238) derivatives. J Med Chem 46:2279–2282

Ritchie CW, Bush A, Mackinnon A, Macfarlane S, Mastwyk M, MacGregor L, Kiers L, Cherny RA, Li QX, Tammer A, Carrington D, Mavros C, Volitakis I, Xilinas M, Ames D, Davis S, Beyreuther K, Tanzi RE, Masters CL (2003) Metal-protein attenuation with iodochlorhydroxyquin (clioquinol) targeting Abeta amyloid deposition and toxicity in Alzheimer disease: a pilot phase 2 clinical trial. Arch Neurol 60:1685–1691

Samadi A, Estrada M, Pérez C, Rodríguez-Franco M, Iriepac I, Moraledac I, Chioua M, Marco-Contelles J (2012) Pyridonepezils, new dual AChE inhibitors as potential drugs for the treatment of Alzheimer's disease: synthesis, biological assessment, and molecular modeling. Eur J Med Chem 57:296–301

Seshadri S, Fitzpatrick AL, Ikram MA, DeStefano AL, Gudnason V, Boada M, DeStefano AL, Gudnason V, Boada M (2010) Genome-wide analysis of genetic loci associated with Alzheimer disease. J Am Med Assoc 303:1832–1840

Singh M, Kaur M, Kukreja H, Chugh R, Silakari O, Singh D (2013) Acetylcholinesterase inhibitors as Alzheimer therapy: from nerve toxins to neuroprotection. Eur J Med Chem 70:165–188

Skrzypek A, Matysiak J, Niewiadomy A, Bajda M, Szymanski P (2013) Synthesis and biological evaluation of 1,3,4-thiadiazole analogues as novel AChE and BuChE inhibitors. Eur J Med Chem 62:311–319

Smith CP, Bores GM, Petko W, Li M, Selk DE, Rush DK, Camacho F, Winslow JT, Fishkin R, Cunningham DM, Brooks KM, Roehr J, Hartman HB, Davis L, Vargas HM (1997) Pharmacological activity and safety profile of P10358, a novel, orally active acetylcholinesterase inhibitor for Alzheimer's disease. J Pharmacol Exp Ther 280:710–720

Sugimoto H (2008) The new approach in development of anti-Alzheimer's disease drugs via the cholinergic hypothesis. Chem Biol Interact 175:204–208

Tai HC, Serrano-Pozo A, Hashimoto T, Frosch MP, Spires-Jones TL, Hyman B (2012) The synaptic accumulation of hyperphosphorylated tauoligomers in Alzheimer disease is associated with dysfunction of the ubiquitin-proteasome system. Am J Pathol 181:1426–1435

Xinga W, Fub Y, Shi Z, Lua D, Zhang H, Hua Y (2013) Discovery of novel 2,6-disubstituted pyridazinone derivatives as acetylcholinesterase inhibitors. Eur J Med Chem 63:95–103

Yan H, Yao PF, Chen SB, Huang ZH, Huang SL, Tan JH, Li D, Gu LQ, Huang ZS (2013) Synthesis and evaluation of 7,8-dehydrorutaecarpine derivatives as potential multifunctional agents for the treatment of Alzheimer's disease. Eur J Med Chem 63:299–312

Yerdelen KO (2012) Solvent-free solid supported and phase transferred catalyzed synthesis of benzaniline derivatives using microwave irradiatıon. Int J Pharm Sci Res 3(1):126–129

Yerdelen KO, Gul HI (2013) Synthesis and anticholinesterase activity of fumaramide derivatives. Med Chem Res 22:4920–4929

Zatta P, Drago D, Bolognin S, Sensi SL (2009) Alzheimer's disease, metal ions and metal homeostatic therapy. Trends Pharmacol Sci 30:346–355